Close Mimicry of Lung Surfactant Protein B by "Clicked" Dimers of Helical, Cationic Peptoids

Michelle T. Dohm,[1] Shannon L. Seurynck-Servoss,[2] Jiwon Seo,[3] Ronald N. Zuckermann,[4] Annelise E. Barron[2,3]

[1] *Department of Chemistry, Northwestern University, 2145 N. Sheridan Road, Evanston, IL 60208-3100*

[2] *Department of Chemical and Biological Engineering, Northwestern University, 2145 N. Sheridan Road, Evanston, IL 60208-3100*

[3] *Department of Bioengineering, Stanford University, W300 James H. Clark Center, 318 Campus Drive, Stanford, CA 94305-5440*

[4] *Biological Nanostructures Facility, Molecular Foundry, Lawrence Berkeley National Laboratory, 1 Cyclotron Road, Berkeley, CA 94720*

Received 15 May 2009; revised 18 August 2009; accepted 10 September 2009
Published online 23 September 2009 in Wiley InterScience (www.interscience.wiley.com). DOI 10.1002/bip.21309

ABSTRACT:

A family of peptoid dimers developed to mimic SP-B is presented, where two amphipathic, cationic helices are linked by an achiral octameric chain. SP-B is a vital therapeutic protein in lung surfactant replacement therapy, but its large-scale isolation or chemical synthesis is impractical. Enhanced biomimicry of SP-B's disulfide-bonded structure has been previously attempted via disulfide-mediated dimerization of SP-$B_{1\text{-}25}$ and other peptide mimics, which improved surface activity relative to the monomers. Herein, the effects of disulfide- or "click"-mediated (1,3-dipolar cycloaddition) dimerization, as well as linker chemistry, on the lipid-associated surfactant activity of a peptoid monomer are described. Results revealed that the 'clicked' peptoid dimer enhanced in vitro surface activity in a DPPC:POPG:PA lipid film relative to its disulfide-bonded and monomeric counterparts in both surface balance and pulsating bubble surfactometry studies. On the pulsating bubble surfactometer, the film containing the "clicked" peptoid dimer outperformed all presented peptoid monomers and dimers, and two SP-B derived peptides, attaining an adsorbed surface tension of 22 mN m^{-1}, and maximum and minimum cycling values of 42 mN m^{-1} and near-zero, respectively. © *2009 Wiley Periodicals, Inc. Biopolymers (Pept Sci) 92: 538–553, 2009.*

Keywords: lung surfactant; surfactant protein B; SP-B; click chemistry; peptoid; dimer; lipid monolayer; pulsating bubble surfactometry; protein-lipid interactions

This article was originally published online as an accepted preprint. The "Published Online" date corresponds to the preprint version. You can request a copy of the preprint by emailing the Biopolymers editorial office at biopolymers@wiley.com

Additional Supporting Information may be found in the online version of this article.

Correspondence to: Annelise E. Barron; e-mail: aebarron@stanford.edu
Michelle T. Dohm and Shannon L. Seurynck-Servoss contributed equally to this work.

Contract grant sponsor: U.S. National Institutes of Health
Contract grant number: 2 R01 HL67984
Contract grant sponsor: U.S. National Science Foundation
Contract grant number: BES-0101195
Contract grant sponsor: Collaborative Research in Chemistry
Contract grant number: CHE-0404704
Contract grant sponsor: U.S. Department of Energy
Contract grant number: DE-AC02-05CH11231

INTRODUCTION

Lung surfactant (LS) is a complex lipid-protein mixture that lines the air-liquid (a/l) interface of vertebrate lungs and varies surface tension (γ, mN m^{-1}) with the volume changes that occur during normal respiration. It reduces the work of breathing, maximizes lung

compliance, optimizes the surface area available for gas exchange, and stabilizes the alveolar network against collapse.[1–4] Surfactant replacement therapy (SRT) is an effective, often animal-derived treatment for infant respiratory distress syndrome (IRDS),[1] which occurs with significant incidence in infants born prior to 32 weeks of gestation, when the lungs are underdeveloped and do not secrete functional LS. Currently, there is no effective treatment for acute respiratory distress syndrome (ARDS), which affects adults after lung injury, infection, and in other instances.[2,3] Because of drawbacks associated with both animal- and synthetically derived SRT formulations,[4–7] a great, innovative opportunity remains to develop a fully functional, biomimetic LS of precisely known composition, that is cost-effective, biostable, and nonimmunogenic, and that minimizes the difficulties of aggregation and protease-degradation associated with using peptides and proteins.

LS comprises by weight ~90% lipids (~75% of which is phosphatidylcholine) and ~10% combined protein, including surfactant proteins SP-A, SP-B, SP-C, and SP-D.[8–10] The three requirements for functional LS are (1) rapid adsorption within one minute to the a/l interface (2), attainment of near-zero γ at expiration, and (3) excellent respreadability of material at the interface during respiration, i.e., multiple continuous cycles of film expansion and compression. Although DPPC (a saturated, zwitterionic phospholipid) films reach near-zero γ upon compression, they fail to adsorb quickly or respread efficiently during cycling. The inclusion of additional, unsaturated or neutral lipids to the film improves respreading but raises the minimum γ reached.[11] It has been established that the two hydrophobic SPs, SP-B and SP-C, are critical for the γ-reducing and stabilizing behavior of natural LS, as they are involved in maintaining lipid organization, transport, and the formation of surfactant-associated reservoirs at the a/l interface.[12–14]

SP-B is a small, highly conserved 79 mer with 10 cationic residues, ~45% helicity, and four to five amphipathic helices that are presumably constrained by three intramolecular disulfide bonds and one intermolecular disulfide bond, the latter promoting homo-dimerization in its natural form.[15–18] No resolved structure is currently available. Extensive research into the in vitro and in vivo biophysical properties of SP-B has revealed that in vivo efficacy is improved when clinical formulations include SP-B, and debatably, in preference to the inclusion of SP-C.[5,19,20] Unfortunately, the unique and highly conserved structural characteristics of SP-B (and SP-C) prohibit practical large-scale isolation or chemical synthesis in a manner that preserves the structural integrity and stability, and hence function, of the protein when bound to lipids.

Logically, the design, synthesis, and characterization of simpler peptide mimics (KL_4)[21] or shorter SP-B fragments ($SP\text{-}B_{1\text{-}25}$, $SP\text{-}B_{53\text{-}78}$)[22–26] have been explored. The latter terminal, surface-active segments are connected via two proximally close disulfide bonds in natural SP-B. This orientation is believed to facilitate transient insertion into the interfacial lipid film by electrostatic and hydrophobic interactions with the lipid head-groups and acyl chains, promoting stability and minimizing loss of material to the hypophase. A peptide mimic, $dSP\text{-}B_{1\text{-}25}$, which links two monomers via a disulfide bond, has been extensively researched, and results have indicated that disulfide-mediated dimerization significantly increased surfactant activity for this peptide.[27–30] Additionally, an *N*-/*C*-terminus construct "Mini-B," which links $SP\text{-}B_{8\text{-}25}$ and $SP\text{-}B_{53\text{-}78}$ with two disulfide bonds, also showed very promising surfactant activity relative to a mixture of the respective monomers, with performance as good as or better than the natural protein.[31,32]

The positive contribution to surfactant activity that is seemingly caused by disulfide-mediated dimerization of SP-B peptide mimics has led to the current investigative study. As previously outlined, poly-*N*-substituted glycines (peptoids) have recently been advanced as promising alternatives to peptide therapeutics because they are able to circumvent protease-susceptibility and irreversibly aggregative tendencies typical of hydrophobic proteins and peptides.[33,34] Briefly, peptoids are synthesized via a standard solid-phase protocol[35] and contain nitrogen-substituted side chain variants of their peptide cousins, rendering the backbone achiral and hydrogen bond donor-deficient. However, through the inclusion of bulky, chiral side chains, sequence-specific peptoids are manipulated to adopt a preferred helical handedness, and can form extremely stable polyproline type I-like helices through steric and electronic repulsions.[36,37] Depending on the side chain properties, peptoids exhibit a pitch of ~6–6.7 Å and ~3 residues per turn.[38,39] Design and characterization of peptoids that mimic the generic structural attributes of relevant antimicrobial or SP-related sequences have confirmed their ability to mimic the structure, form, or function of the peptides.[40–45]

This begs the question as to whether a previously characterized peptoid that mimics the helicity, amphipathicity, and hydrophobicity of the *N*-terminus of SP-B will exhibit enhanced in vitro surface activity upon dimerization.[41–43] We report here the design, synthesis, and in vitro characterization of five dimerized peptoids. Four of these are dimerized using a disulfide linkage: one via the secondary amine at the *N*-terminus, and three others at the *C*-terminal end, flanked by an achiral octamer spacer of varying hydrophobicity. The fifth dimer replicates one of the dimers with a *C*-terminal linker, but the linkage is formed through "click-chemistry" (1,3-dipolar cycloaddition) instead of a disulfide bond.[46,47]

The "click-chemistry" triazole-containing linkage has been shown to impart desired pharmacologic properties and activities to a variety of molecules.[48–50] To assess in vitro surface activity in a "Tanaka lipid" film (TL)[51]: 1,2-diacyl-*sn*-glycero-3-phosphocholine (DPPC): 1-palmitoyl-2-oleoyl-*sn*-glycero-3-[phospho-*rac*-(1-glycerol)] (POPG): palmitic acid (PA) 68:22:9 by weight, all peptoids were characterized using a Langmuir-Wilhelmy surface balance (LWSB) equipped with epifluorescent microscopic (FM) imaging and a pulsating bubble surfactometer (PBS). Monomeric variants of the dimers, with and without a linker, were also characterized for comparative purposes. For relevant techniques, the dimers and monomers were compared to established, previously characterized peptide mimics of SP-B (KL_4 or SP-$B_{1\text{-}25}$).

In this study, we find that disulfide-mediated dimerization led to little or no improvement in peptoid surface activity relative to the monomer. Enhanced surface activity depended on the side chain chemistry and presence of the linker. However, "click"-mediated dimerization significantly improved in vitro surface activity, seemingly by imparting conformational rigidity and polarity to the structure. The activity characteristics of the "clicked" dimer match and even excel relative to those of current peptide mimics. This work represents the first instance of biophysical activity by a "clicked" peptoid,[47] and may influence future peptide- and/or peptoid-based dimer designs.

RESULTS

Mimic Design Rationale

The primary motivation for investigating peptide- or peptoid-based molecules as substitutes for SP-B in an LS formulation is the mounting evidence that SP-B plays a vital role in LS biophysical function. Unfortunately, SP-B is inaccessible in pure form on a large scale for use in a synthetic formulation. Replacing SP-B (or SP-C) with a fully functional molecule in a biomimetic formulation may result in a more bioavailable, cost-effective, and safer alternative than the currently used, animal-derived counterparts. To date, lone amphipathic peptide helices as SP-B mimics have failed to reproduce the behavior that results from the protein's naturally more complex structure; although select peptides have shown very promising in vitro and in vivo LS activity, none have been introduced to the pharmaceutical market.[52,53] As a result, disulfide-mediated dimerization of peptide mimics has been extensively investigated in an attempt to enhance the biomimicry of SP-B's sequence and structure. In particular, dSP-$B_{1\text{-}25}$ and Mini-B significantly improved surfactant performance in both in vitro and in vivo tests when compared to their respective monomers.

Earlier generations of single helix peptoid-based SP-B mimics have displayed in vitro surface activity as good as or better than the SP-$B_{1\text{-}25}$ and KL_4 peptides.[41–43] The previously designed and characterized 17mer **B1** (Figure 1) mimics the helicity, hydrophobicity, and cationic facial amphipathicity of both peptides, with particular attention paid to including the fewest number of different residues, the latter similar to KL_4. Inclusion of bulky, chiral, and aromatic (*N*spe, Phe-like) side chains in peptoids has increased in vitro surface activity relative to sequences with chiral, aliphatic (*N*ssb, Ile-like) side chains.[41,42] In the present work, the five dimerized peptoids presented in Figure 1 elaborated on the **B1** sequence by exploring new avenues of SP-B biomimicry in non-natural oligomers.

Peptoid **dB1** is a simple, *N*-terminally disulfide-bonded dimer of **B1**, which mimics one of the *N*-/*C*-terminus intramolecular disulfide bonds that naturally exists between SP-$B_{1\text{-}25}$ and SP-$B_{53\text{-}78}$. Peptidomimetic analogs **dB2**, **dB3**, and **dB4** were also dimerized via a disulfide bond, but at their *C*-termini, and possess extended peptoid sequences, comprising an octameric bridging region that is primarily hydrophilic and achiral. The location of this disulfide bond mimics the intermolecular bond that homodimerizes two SP-B monomers, i.e., located positionally opposite the dimerized *N*-/*C*-terminus region. The octameric chain, which includes two four-residue segments that flank the disulfide bond, loosely mimics the SP-$B_{23\text{-}54}$ peptide segment, which also flanks the intermolecular disulfide bond in the natural protein. In this SP-B segment, >60% of the residues exhibit hydrophilic or mildly hydrophobic properties, with interspersed hydrophobic residues. In addition, large stretches of amino acids without a disulfide bond are present, implying a less structurally constrained region.

Therefore, the hydrophobicity of four (50%) of the side chains in the octameric linker region were increased for each molecule, comprising *N*meg, *N*prp, or *N*pm in **dB2**, **dB3**, and **dB4**, respectively (Figure 1). Linker regions of varying side chain hydrophobicity may facilitate different degrees of interaction with the lipid film at the a/l interface, or may promote intra- or intermolecular association between two helices of the same or different units, respectively. Note that the extent of helicity of **B1**, previously reported,[41,42] is stabilized in peptoids through steric and electronic repulsions, and therefore, the addition of a *C*-terminal linker region that is primarily achiral would be expected to slightly reduce the helical signal, but have little to no effect on the secondary structure of the main peptoid helix (see Figure 1 SI).

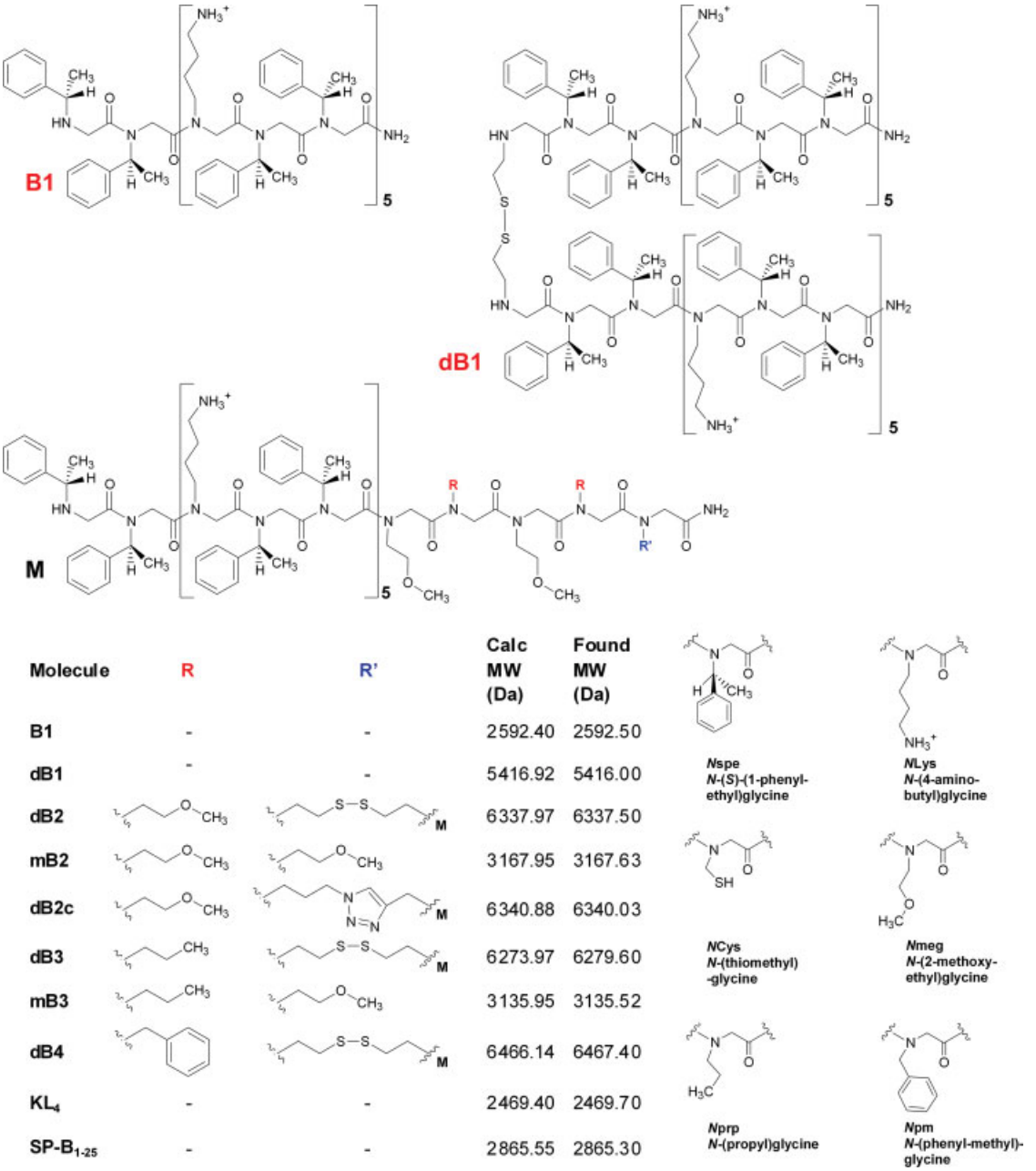

FIGURE 1 Peptoid Mimic Chemical Structures and Molecular Weights. **B1** is the designated, original peptoid helix monomer. **dB1** is the simple dimer linked by a disulfide bond at the *N*-terminus. **M** designates the monomer + linker unit of varying side chain properties that also represents half of the dimers **dB2-4**. **R** and **R'** substituents are listed in the table for each molecule. Monomers **mB2** and **mB3** contain an *N*Cys → *N*meg substitution at the *C*-terminus, while dimers **dB2**, **dB3**, and **dB4** are *C*-terminus linked by a disulfide bond. In **dB2c**, **R'** is composed of a triazole linkage that is created via 'click-chemistry'. Found molecular weights were obtained by either ESI/MS or MALDI-TOF/MS.

To further explore the effect of dimer linkage on surfactant activity, azide- and alkyne-containing monomers of **dB2** were conjugated via 1,3-dipolar cycloaddition, or "click-chemistry" to form **dB2c** (Figure 1). The 1,4-disubstituted triazole ring has been shown to impart physiochemical stability and rigidity to different structures.[48] For comparative purposes, monomer variants of **dB2** and **dB3** were synthesized (**mB2** and **mB3**), with an *N*Cys→*N*meg substitution at

the *C*-terminus (Figure 1) to prevent unwanted dimerization. Where applicable, peptoids were compared with the established peptide mimics SP-$B_{1\text{-}25}$ and/or KL_4.

LWSB Studies: Pressure-Area Isotherms

LWSB experiments, performed at 25 and 37°C, yielded surface pressure (Π, mN m^{-1}) - molecular area (Å^2 $molec^{-1}$, or A) isotherms for films spread at the a/l interface. Such isotherms characteristically exhibit a high (early) 'liftoff' area, the A at which Π first measurably increases from zero, a progression from the liquid-expanded (LE) to liquid-condensed (LC) phases, and finally, to a high collapse Π of $\geq$70 mN m^{-1} or near-zero γ. In addition, a pronounced, extended plateau often occurred at $\sim$40–50 mN m^{-1}. The first two characteristics correspond to the first two criteria for a functional LS film, i.e., a γ-reducing effect at the a/l interface (liftoff at a large film surface area), and reaching near-zero γ at compression (a high collapse pressure). It should be noted that although the liftoff feature is outside the physiologically relevant surface pressure regime for lung surfactant function ($\geq$40 mN m^{-1}), it is a useful indicator for determining the γ-reducing effect in the presence of the surface-active additive, and for estimating similarity to the behavior of SP-B.[29]

The third characteristic, an extended plateau in the isotherm, has a significance that is well-debated, but is believed to represent a phase transition corresponding to reversible squeeze-out of material (possibly of specific molecules) from the monolayer into associated surfactant reservoirs below the surface. This plateau may be related to respreadability and is a defining characteristic for the behavior of SP-B, SP-C, and mimics thereof, in the presence of lipids. Though the plateau size is a compression rate-dependent property, under the same compression rate, the relative plateau shapes, and sizes of the lipid-peptoid films can be compared to that of the lipid-only film.

Lipid-peptoid isotherms, regardless of temperature, exhibited a high collapse $\Pi \geq$ 70 mN m^{-1} (Figure 2) which is mimetic of SP-B in this lipid mixture,[29] and of the natural LS film. For average liftoff data and 2D isotherm features $\pm$ standard deviation of the mean (σ), see Table I. At both temperatures, the Tanaka lipid (TL) film exhibited a later liftoff (lower molecular area) and smaller plateau than any of the lipid-peptoid films (93 Å^2 $molec^{-1}$ at 25°C, 101 Å^2 $molec^{-1}$ at 37°C, see Table I). At 25°C (Figure 2A and 2B), **TL + B1** and + **dB1** (the linker-free dimer of **B1**) had nearly overlapping isotherms, as did most of the other monomer/dimer pairs with the exception of the *N*propyl-containing pair (**TL + mB3/dB3**) and the purely *N*meg-containing "clicked" dimer, relative to its monomer (**TL + mB2/dB2c**).

Although **TL + mB2** had an earlier liftoff than the film containing its disulfide-linked dimer **dB2**, the gradual slope rendered the difference unnoticeable in this regime, while the film containing the clicked variant **dB2c** had a significantly later liftoff. **TL + dB4** (*N*pm-containing linker), while not shown, exhibited an isotherm that directly overlaid that of **TL + B1**. **TL + dB3** (*N*propyl) had the earliest liftoff, even above the film containing its monomer (**mB3**), while the **dB2c**-containing film had the latest (Table I). At a compression rate of 30 mm min^{-1}, the plateau sizes were similar for all films except for the *N*propyl-containing pair (**TL + mB3/dB3**), for which they were the longest in A (Table I). Notably, the isotherm shapes were different for this pair, where the lipid-dimer isotherm had a steeper slope and is therefore considered less compressible than the lipid-monomer film.

In a more fluid lipid film at a more physiologically relevant temperature, 37°C (Figure 2C and 2D), all isotherms exhibited earlier liftoffs and more pronounced plateaus than at 25°C. Interestingly, with the exception of **TL + dB2c**, all of the lipid-dimer isotherms had earlier liftoffs than their respective lipid-monomer isotherms (Table I). Again, the film containing the dimer with *N*propyl chains, **TL + dB3**, possessed the earliest liftoff and longest plateau, where an early liftoff and pronounced plateau are considered desirable surface activity characteristics that mimic SP-B in this lipid mixture.[29] The film with the clicked dimer (**TL + dB2c**) had a nearly overlapping isotherm with the lipid-monomer variant film, and as at 25°C, **TL + dB4** (*N*pm-containing, not shown) exactly overlaid **TL + B1**.

According to the listed criteria for functional LS, any one of these molecules could be a considered a good, surface-active mimic of SP-B. However, subtle but significant differences in surface activity characteristics lend more insight into the mechanics of these lipid-peptoid films. The addition of a peptoid + linker (**mB2**) did little to improve activity relative to **B1**. Dimerization and linker hydrophobicity had a much more significant effect on surface activity, primarily at 37°C. *N*-terminal dimerization (**dB1**) with no linker did improve surface activity relative to the monomer, and *C*-terminal dimerization with the addition of a hydrophilic linker containing 50% aliphatic properties (**dB3**) seemed to have the optimal effect. To further evaluate the surface activity of these films, the FM film morphology was examined.

LWSB Studies: Epifluorescent Microscopy of Lipid-Peptoid Films

FM images were recorded at 25 and 37°C on a Langmuir trough with 0.50 mol% Texas Red DHPE (TR-DHPE) spiked into the solution containing lipids or lipids + peptoid

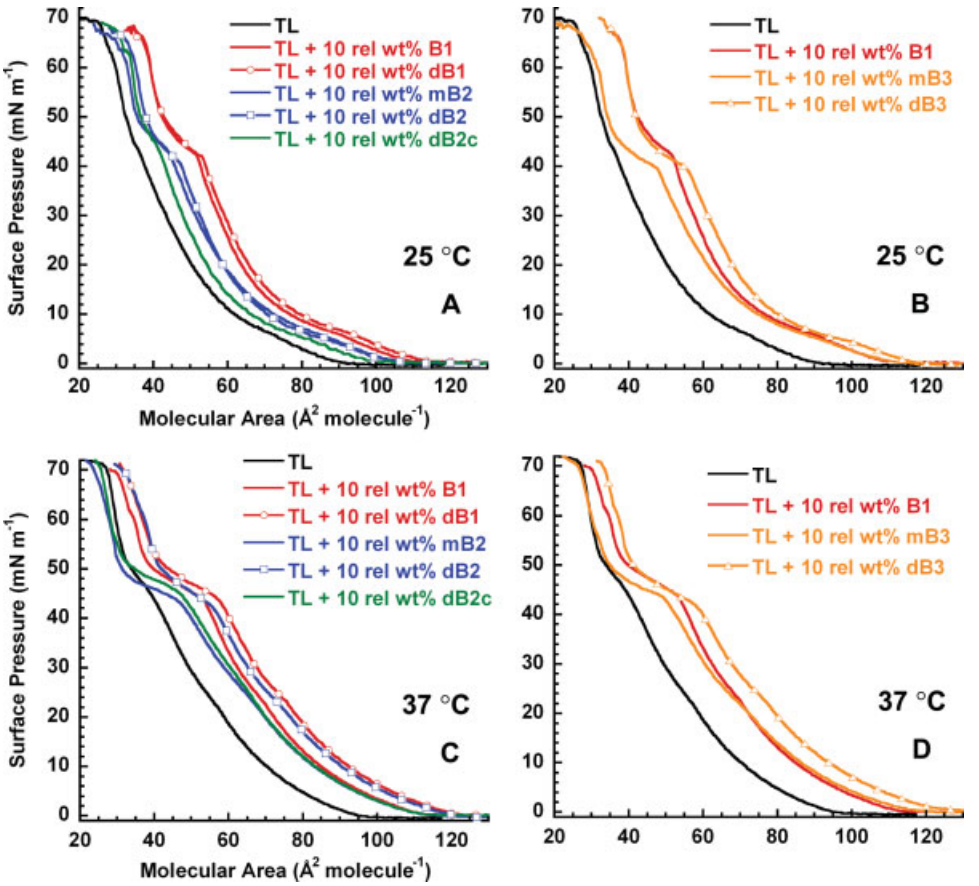

FIGURE 2 LWSB Surface Pressure (Π) - Molecular Area (A) Isotherms at 25 and 37°C. Π-A isotherms of films are representative first compressions on aqueous buffer (150 mM NaCl, 10 mM HEPES, 5 mM $CaCl_2$, pH 6.9) with a unidirectional barrier speed of 30 mm min^{-1}. Tanaka lipids alone (**TL**, black), **TL** +10 relative wt% **B1** (red), + **dB1** (red, open circles), + **mB2** (blue), + **dB2** (blue, open squares), + **dB2c** (green), + **mB3** (orange), + **dB3** (orange, open triangles) at 25°C (Panels A and B) and 37°C (Panels C and D). **TL** +10 relative wt% **dB4** was omitted for clarity, but directly overlaid **TL +10 relative wt% B1**. See Table I for mean values ± σ of isotherm 2D phase transition markers.

(Figure 3). TR-DHPE is a bulky, fluorescently headgroup-labeled lipid that is preferentially excluded from the more ordered regions of the monolayer upon film compression. Therefore, dark regions of the monolayer represent LC domains, while lighter regions correspond to the more fluid LE phase. Bright spots present in images may represent sub-monolayer vesicles or protrusions above the monolayer that are still associated with the film, and are termed here bright protrusions. It is not known whether bright protrusions contain a higher proportion of dye, or are folds with a multi-component composition; they are simply considered to be pockets of material removed from the monolayer.

FM images are presented at Π that correspond to before and after the plateau region at both temperatures: 41 and 51 mN m^{-1} at 25°C (Figure 3, left image set), and 42 and 54 mN m^{-1} at 37°C (Figure 3, right image set). For these films, LC domains formed at 3–7 mN m^{-1} at 25°C and 25–30 mN m^{-1} at 37°C; bright protrusions, if formed, occurred at 42–48 mN m^{-1} at both 25°C and 37°C. At 41 mN m^{-1} at 25°C, the **TL** film contained LC domains surrounded by the brighter fluid LE phase. This morphology was mostly consistent for all of the lipid-peptoid films, where **TL** + **mB2/dB2/dB2c** had slightly smaller domains than **TL**, while **TL** + **mB3/dB3** had slightly larger domains, and **TL** + **B1** and **TL** + **dB4** had very similarly sized domains to **TL**. Upon closer inspection, small bright protrusions were observed in **TL** + **dB3** and **TL** + **dB2c**.

Interestingly, at 25°C, the bright protrusions in **TL** + **dB2c** were seemingly located in or on the center of the LC domains. At 51 mN m^{-1}, the **TL** film contained LC domains of roughly the same density as at 41 mN m^{-1}, but with the additional inclusion of small bright protrusions. However,

Table I LWSB Isotherm 2D Phase Transition Markers

Film	25.0 ± 0.3°C					37.0 ± 1.5°C				
	Liftoff	Kink		Plateau Length		Liftoff	Kink		Plateau Length	
	(A[a])	(A)	(Π[b])	(A)	(Π)	(A)	(A)	(Π)	(A)	(Π)
TL[c]	$93_{(3)}$	68	7	3	7	101	55	24	8	8
TL + B1[d]	114	93	5	9	8	118	68	25	18	9
TL + dB1	117	92	6	$12_{(3)}$	11	124	72	24	19	13
TL + mB2	119	88	$7_{(2)}$	12	8	116	67	23	17	10
TL + dB2	110	88	6	9	9	$125_{(3)}$	72	24	16	11
TL + dB2c	106	$76_{(4)}$	6	7	10	$118_{(7)}$	64	26	$17_{(5)}$	10
TL + mB3	117	87	6	13	10	$123_{(5)}$	67	23	$18_{(3)}$	12
TL + dB3	121	98	5	13	10	128	76	24	20	13
TL + dB4	119	93	6	$11_{(2)}$	10	117	70	23	15	11
σ[e]	≤2	≤3	≤1	≤1	1	≤2	≤3	≤2	≤2	≤2

[a] Mean molecular area expressed in Å^2 per molecule.
[b] Mean surface pressure expressed in mN m^{-1}.
[c] Tanaka lipid mixture, DPPC:POPG:PA 68:22:9 [wt].
[d] Mimics added at 10 wt% relative to the total lipid content.
[e] For clarity, the standard deviation of the mean (σ) for each type of value is collectively reported at the base of the column, with exceptions in the table listed as "$a_{(b)}$," where a is the mean and b is the σ.

depending on the run, these bright protrusions were sometimes very sparse or seemingly not present. All of the lipid-peptoid films contained LC domains that were roughly the same size and density as those observed at 41 mN m^{-1}. The major differences in film morphology were thus in bright protrusion formation and patterning, which for **TL + dB1**, **TL + dB2**, and **TL + dB4**, were very sparse or absent. Lipid-monomer films (**TL + B1**, **TL + mB2**, and **TL + mB3**) all exhibited bright protrusions, with most prevalence in the **TL + mB3** film. **TL + dB3** and **TL + dB2c** were the only lipid-dimer films that exhibited a significant amount of bright protrusions at this lower temperature. Although **TL + dB2c** bright protrusions were more sparse, their location in the center of the LC domains was more distinctly observed at 51 mN m^{-1}.

At 37°C, the domain boundaries in the FM images became less clear as they were more difficult to capture due to increased *x-y* translational movement (in-plane) of the more fluid film (Figure 3). At 42 mN m^{-1}, the same trend in LC domain size was observed as at 25°C. One notable difference was that for **TL + dB2c**, elongated rod-like shapes formed in addition to circular LC domains. These rod-like shapes are sometimes seen in the imaging of giant unilamellar vesicles (GUV's), and have been established as evidence of a more fluidized film.[54] At 54 mN m^{-1}, LC domains nearly disappeared in all lipid-monomer films, and for **TL + dB4**. Bright protrusions were present in all films, where the patterning was, in some cases, quite distinct. **TL + B1** displayed very small, bright protrusions, whereas **TL + dB1** had duller, larger bright protrusions. While **TL + dB2** had sparse, bright protrusions, its lipid-monomer variant film (**TL + mB2**) displayed many more, larger, duller bright protrusions. Interestingly, **TL + dB2c** bright protrusions were either bright and sparse, or were duller and seemed to lie directly on the rod-like structures. **TL + mB3/dB3** both had a tremendous amount of small, bright protrusions.

By correlating isotherm features with FM images, a better in vitro surface activity assessment for this technique is provided. Relating structure to function, *N*-terminal, simple dimerization did not significantly alter the phase morphology, and *C*-terminal dimerization resulted in morphology changes dependent on linker hydrophobicity. From the isotherms, the most surface-active films would be **TL + mB3** or **TL + dB3**, and FM images revealed a possible cause for this increase in activity. An easily compressed, easily respread monolayer would likely display homogeneously sized, small LC domains that coexist with small bright protrusions at high Π. This promotes elasticity and facile reorganization of the monolayer into highly compressed states. Small bright protrusions are more likely to easily re-spread than larger sub- or super-monolayer structures, and for these two films, this was exactly observed. Note that the presence of a plateau region does not necessitate the presence of bright protrusions. A lack of bright protrusions may point to inferior surface activity or an inefficient mechanism of folding to accommodate higher surface pressures.

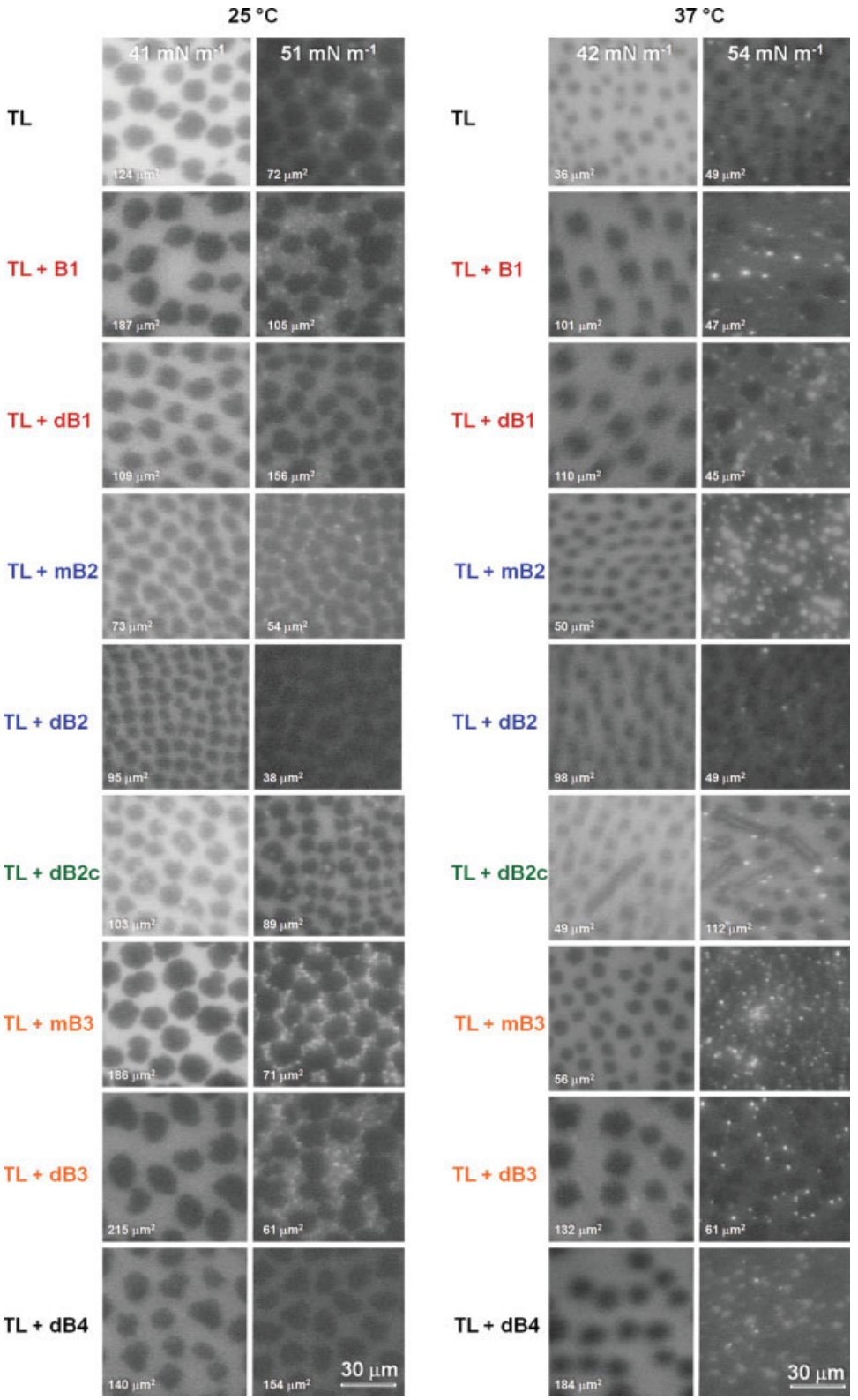

FIGURE 3 FM Images of Lipid Phase Morphology on the LWSB at 25 and 37°C. Representative epifluorescent microscopic images for Tanaka lipids alone (**TL**) and TL +10 relative weight % of each mimic on aqueous buffer (150 mM NaCl, 10 mM HEPES, 5 mM $CaCl_2$, pH 6.9) are presented at 41 and 51 mN m^{-1} at 25°C (left image set) and 42 and 54 mN m^{-1} at 37°C (right image set). Films were compressed at a barrier speed of 5 mm min^{-1}. Average LC domain sizes are listed in the lower left corner of each subpanel.

The frequency and density of bright protrusions coexisting with LC domains indicates that material was evenly removed, but still associated with, the interfacial monolayer, and may be re-spread upon expansion. Although not shown, all LC domains and bright protrusions disappeared with expansion of the compressed film. Surprisingly, the type of dimerization did seem to affect the phase morphology, where the most distinct patterning was observed with **TL + dB2c**. The unique shape of the LC domains and localization of bright protrusions indicates that the mechanism of material removal and reorganization upon film compression may be somewhat different in this case.

Pulsating Bubble Surfactometry: Static Mode

The adsorption kinetics of the lipid-peptoid aqueous suspensions were studied using the PBS at 37°C in static mode, which monitors γ over time (Figure 4A). A clinically administered LS formulation, Infasurf®, adsorbed rapidly to the interface in less than one minute, and attained a low equilibrium γ (γ_{eq}) of ~23 mN m^{-1} or less on the PBS.[55] Rapid adsorption to the a/l interface is one of the key criteria in LS biophysical functioning. The adsorption curves for lipid-peptoid films are presented in Figure 4, and the average γ data $\pm$ σ at selected time intervals, in comparison to SP-B$_{1\text{-}25}$ and KL$_4$, is available in the Supporting Information (Table II SI). The **TL** film adsorbed quite slowly to the interface, requiring nearly 20 min to reach a high γ_{eq} of ~54 mN m^{-1}. All lipid-peptoid films improved upon these adsorption characteristics, but to significantly different extents. **TL + B1/dB1** reached relatively similar γ_{eq} values (39 and 41 mN m^{-1}, respectively), but **TL + dB1** adsorbed to this value much more quickly than **TL + B1**. **TL + mB2** promoted more rapid adsorption to a significantly lower γ_{eq} than **TL + dB2** (40 and 46 mN m^{-1}, respectively). **TL + dB2c** reached a dramatically lower γ_{eq} of 22 mN m^{-1}, which nearly matched that of KL$_4$ and Infasurf®,[55] albeit at a slower adsorption rate. **TL + mB3/dB3** adsorbed at more rapid rates and reached similar γ_{eq} values (37 and 38 mN m^{-1}, respectively), which were improved over any of the other disulfide-bonded dimers or their monomeric counterparts. **TL + dB4**, although not shown, adsorbed more rapidly than **TL + B1**, but reached a significantly higher γ_{eq} of 46 mN m^{-1} (Table II SI). Even with slower adsorption—reaching γ_{eq} in 5 min—the **TL + dB2c** film demonstrated superior adsorption characteristics relative to the other lipid-peptoid films.

Pulsating Bubble Surfactometry: Dynamic Mode

Perhaps the most physiologically relevant in vitro test for any LS formulation is the endurance of the film at the a/l interface during rapid changes in volume or surface area. Running the PBS in dynamic mode allows for a simplified evaluation of film behavior under such conditions. The γ-surface area (SA, mm^2) data loops for each lipid-peptoid film, shown in Figure 4B–4C, represent one pulsation cycle at 20 cycles per minute (cpm) after 5 min, with expansion in a clockwise loop direction. The average $\gamma_{max/min}$ data $\pm$ σ at selected time intervals, in comparison to SP-B$_{1\text{-}25}$ and KL$_4$, is presented in Table II. Low γ data is absent, i.e., difficult to obtain, in some loops due to the inability of the image analysis system to trace bubble shape in this regime. At low γ, the lipid film is in a highly compressed state, and the bubble shape often deforms significantly from that of an ellipse or sphere, where the ellipsoidal Laplace equation is normally used to calculate γ and SA based on a trace of bubble shape and voltage data from the instrument. Regardless, it was clear from data analysis and visual, real-time inspection that γ reached near-zero in these films. Additionally, bubble size was not uniform for every experiment, but differences in absolute surface area (positioning on the *x*-axis, Figure 4) had no appreciable effect on γ as long as data could be accurately traced.

Maintaining a reduced γ throughout respiration, and importantly, near-zero γ upon film compression, are key features of LS that indicate film stability and respreadability. The PBS loop for Infasurf®[55] is known to have a maximum $\gamma(\gamma_{max})$ of ~35 mN m^{-1} and a minimum $\gamma(\gamma_{min})$ near zero; near-zero γ_{min} must be attained immediately upon cycling and should remain for an extended period with minimal compression. Although the significance of bubble hysteresis has not been established, a large amount of hysteresis often correlates with a low amount of compression to reach near-zero, which is a very desirable characteristic in LS formulations. The **TL** film exhibited a high γ_{max} ~ 63 mN m^{-1} and γ_{min} ~ 10 mN m^{-1}, with ~ 44% compression (Figure 4, inset table, and Table II).

The addition of any one of the peptoid-based SP-B mimics to the lipid film resulted in a γ_{min} near zero immediately at cycling commencement, a decrease in γ_{max}, and a reduction in percent compression. The near-zero γ_{min} is expected given the presence of this feature in previous characterization of **TL + B1** films.[41–43] Although **TL + B1/dB1** exhibited similarly shaped loops, **TL + dB1** reached a higher γ_{max} (57 mN m^{-1} relative to 52 mN m^{-1}) and had an increased percent compression (39% relative to 31%). This trend was followed for every monomer/disulfide dimer pair, where the γ_{max} was higher and percent compression increased (Table II). **TL + dB4**, although not shown, displayed activity and a loop shape very similar to **TL + dB2**. Of the disulfide-bonded dimers, **TL + dB3** had the lowest γ_{max}

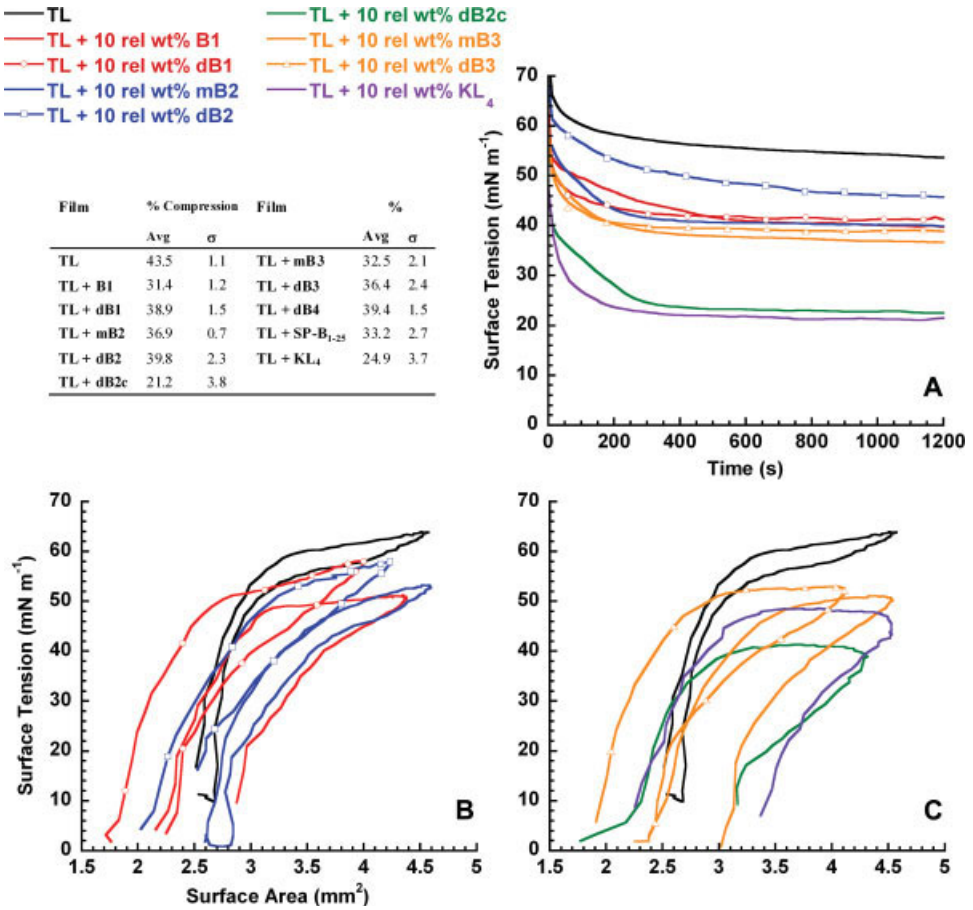

Film	% Compression Avg	σ	Film	% Avg	σ
TL	43.5	1.1	TL + mB3	32.5	2.1
TL + B1	31.4	1.2	TL + dB3	36.4	2.4
TL + dB1	38.9	1.5	TL + dB4	39.4	1.5
TL + mB2	36.9	0.7	TL + SP-B_{1-25}	33.2	2.7
TL + dB2	39.8	2.3	TL + KL_4	24.9	3.7
TL + dB2c	21.2	3.8			

FIGURE 4 PBS Data for Lipid-Peptoid Films in Static and Dynamic Modes at 37°C. Representative static (Panel A) and dynamic (Panels B and C) data for Tanaka lipids alone (**TL**, black), **TL** +10 relative weight % **B1** (red), + **dB1** (red, open circles), + **mB2** (blue), + **dB2** (blue, open squares), + **dB2c** (green), + **mB3** (orange), + **dB3** (orange, open triangles), + **KL_4 peptide** (purple) in aqueous buffer (150 mM NaCl, 10 mM HEPES, 5 mM $CaCl_2$, pH 6.9) at 37°C. **TL** +10 relative wt% **dB4** was omitted for clarity. In dynamic cycling, bubble expansion is clockwise from left to right, and vice versa for compression. Inset table presents the average % surface area (SA) compression ± σ required to reach 20 mN m^{-1} for each molecule. See Table II for average dynamic cycling data ± σ at 20 cpm and Table II SI for average adsorption data ± σ.

(53 mN m^{-1}) and percent compression (36%), and of the monomers, **TL + mB3** was the most surface-active, with a slightly lower γ_{max} and about the same percent compression as **TL + B1**. However, the **TL + dB2c** film surprisingly demonstrated superior in vitro surface activity relative to all other dimers, monomers, and the KL_4 peptide, with a γ_{max} of 42 mN m^{-1} and 21% SA compression to reach 20 mN m^{-1}.

These results indicate that *N*-terminal disulfide-based dimerization of peptoids without a linker renders little benefit to dynamic surface activity characteristics in a mixed lipid film. This is in direct contrast to the single disulfide-bonded dSP-B_{1-25}, which was reported to be significantly more surface-active than the monomer. However, inclusion of a ≥50% hydrophilic linker region at the *C*-terminus in peptoids did yield some benefit, which depended on side chain chemistry and not dimerization. The molecules that possessed 50% aliphatic residues, **mB3** and **dB3**, performed the best in their respective classes (monomer and dimer). Interestingly, with the exception of **dB3**, the addition of a disulfide-based dimer to the lipid film resulted in inferior surface activity relative to all of the monomers, including the original monomer **B1**. However, a dramatic improvement was witnessed when a peptoid dimerized via "click-chemistry" was added to the lipid film, resulting in dynamic film surface activity characteristics that surpass all other peptoids and both single helix peptide mimics KL_4 and SP-B_{1-25}.

Table II PBS Cycling Data at Selected Time Intervals, 20 cpm, 37°C

	1 min		5 min		10 min	
Film	γ^{a}_{max}	γ_{min}	γ_{max}	γ_{min}	γ_{max}	γ_{min}
TL	64.4[c]	$13.1_{(3.5)}$	63.4	10.1	62.7	10.1
TL + B1[b]	51.6	<1	51.6	<1	51.6	<1
TL + dB1	55.1	<1	57.1	<1	56.8	<1
TL + mB2	53.7	<1	53.9	<1	52.6	<1
TL + dB2	60.2	<1	60.0	<1	54.7	<1
TL + dB2c	42.4	<1	41.9	<1	42.4	<1
TL + mB3	50.8	<1	51.1	<1	50.8	<1
TL + dB3	53.1	<1	52.6	<1	52.9	<1
TL + dB4	57.6	<1	58.4	<1	59.0	<1
TL + SP-B_{1-25}	49.6	<1	49.9	<1	49.8	<1
TL + KL_4	47.2	<1	48.7	<1	48.2	<1

[a] Mean surface tension expressed in mN m^{-1}.
[b] Mimics added at 10 wt% relative to the total lipid content.
[c] All σ values were 0.4–2.2 mN m^{-1} unless otherwise denoted. No σ values are available for "<1" table entries.

DISCUSSION

In this study, we explored the effects of dimerization and linker hydrophobicity on in vitro surface activity of peptoid-based mimics of SP-B in a mixed lipid film. The presence of multiple disulfide bonds in natural SP-B facilitates the in vitro and in vivo surface activity that enables the lung's biophysical function. Three intramolecular disulfide bonds, two connecting the *N*-/*C*-terminus segments, and an additional one further along in the sequence, constrain the secondary structure and flexibility of the protein when bound to lipids. For SP-B homodimers in a surfactant film, the intermolecular disulfide bond is postulated to act as a hinge, effectively anchoring, organizing, and inserting squeezed-out lipid assemblies to and from the monolayer at the alveolar interface. This activity is believed to be vital for efficient respreading of material throughout the alveolar area cycling that occurs during breathing.

Whether these disulfide bonds are absolutely required for protein function has been extensively studied, but their exact contributions to molecular structure and function in vivo remain unknown. Although chemically synthesized SP-B_{1-78} has exhibited good in vitro surface activity, it was still inferior when compared to the naturally isolated protein.[29,56] Biophysical functioning of natural SP-B was inhibited if the protein was completely reduced,[57] or if homo-dimerization was prohibited transgenically or through the position-specific substitution of Cys48 → Ser in the sequence.[58,59] Although totally reduced forms of natural SP-B demonstrated surface activity, the protein behaved in a manner that is congruent with increased structural flexibility.[57]

Further evidence that supports the necessity of dimerization is the propensity of SP-B and other saposin-like proteins to form a buried hydrophobic cavity.[60,61] This cavity has been postulated to partake in lipid binding events that aid in the lipid transport and reorganization at the interface during respiration. This buried domain may form during oligomerization or through hydrophobic and hydrophilic associations between SP-B monomers, but disulfide bonds likely ensure the presence of this cavity through conformational restrictions.

This study elucidates possible differences between the mechanisms of surface activity in peptide and peptoid mimics of SP-B. Whereas disulfide-mediated dimerization of SP-B_{1-25} near the *N*-terminus resulted in improved surface activity in vitro and in vivo when compared to the monomer,[27] peptoids were significantly less affected. Interestingly, on the trough at 37, but not 25°C, disulfide-bonded dimers exhibited earlier (higher) liftoff areas than the monomers. In the more fluid film at an elevated temperature above the T_c of the lipid mixture, more peptoid dimer may have been able to insert into the interfacial monolayer than at lower temperature, thus decreasing the available space per molecule at the interface. Because the dimers are roughly twice as large as the monomers, this may have translated to an earlier liftoff at a higher area per molecule. However, a seemingly opposite trend in surface activity was observed on the PBS at 37°C, where the monomers tended to have faster adsorption rates and lower γ_{eq}, in addition to a lower γ_{max}, than the disulfide-based dimers. Because the LWSB is a quasi-equilibrium, slow-cycling technique, isotherm features cannot always be directly correlated to adsorption and cycling features on the PBS. In the rapidly cycled dynamic film on the PBS, it appears that disulfide-mediated dimerization may have actually hindered surfactant activity in peptoid mimics. Thus, for disulfide-based peptoid mimics, it appears that early liftoff areas do not always correlate directly with an increase in surface activity observed when using more physiologically relevant techniques.

As SP-$B_{Cys48 \rightarrow Ser}$ monomers have been shown to associate as dimers non-covalently,[59] which contributed favorably to their activity, mimicking the natural sequence, there exists some evidence that peptoid oligomerization of "monomer" (helix) units can occur in salt solution through associations of the aromatic side chains (Yoriel Marcano, Annelise E. Barron, unpublished work). This phenomenon could explain the lack of improvement observed with disulfide-mediated dimerization of **B1**. If close proximity of the two peptoid helices to each other is the most important factor in contributing to surface activity, and extensive peptoid oligomerization

is already occurring, disulfide-mediated dimerization could be unnecessary, or, as observed on the PBS, inhibiting. Translating to the biophysical function of lung surfactant, an underlying mechanism of aromatic peptoid–peptoid intermolecular associations at the a/l interface may promote sufficient film organization/folding and lipid transport during surface area expansion and compression, rendering a simple disulfide bond of little benefit.

Although mostly excluded from peptide mimic sequences, the >60% hydrophilic residues in SP-$B_{23\text{-}54}$ may also play a critical role in lipid insertion and organization at the a/l interface.[62] By introducing an achiral, octameric peptoid chain with ≥50% hydrophilic residues at the *C*-terminus of **B1** in mB2 and mB3, we attempted to mimic this portion of the protein. Results indicated that the in vitro surface activities of each of the peptoids in the lipid film depended more on the side chain chemistry of the linker than on *C*-terminal, disulfide-mediated dimerization.

Differences in the phase morphology of lipid-peptoid films were attributed mostly, to linker hydrophobicity and not disulfide-mediated dimerization. At lower temperature and higher Π, the lack of surface activity in the disulfide-bonded dimers, except for **dB3**, was clearly observed, where inclusion into the lipid film did not result in bright protrusion formation, which was not the case for inclusion of any monomer. The absence of bright protrusions despite the presence of a plateau region in these films could result from a different mechanism of material removal that is less efficient for reaching near-zero surface tensions and subsequent respreading. This may translate physiologically to increased respreading upon film expansion (inhalation) and increased formation of sublayer structures at compression (expiration). Only the presence of **mB3** and **dB3** resulted in extensive bright protrusion formation, which corroborated the increased activity observed in the isotherms (early liftoff and an extended plateau) in this Π regime.

However, at higher temperature and higher Π, the disulfide-based dimers became more surface-active, as indicated by extensive bright protrusion patterning in all cases. Although again, only the inclusion of *N*-propyl chains in **mB3** and **dB3** resulted in the desired formation of homogeneous and small bright protrusions with high density and frequency. This result further supports the idea that *N*-propyl chains are able to facilitate hydrophobic interactions with other peptoid residues, or partially insert into and associate with the lipid acyl chains at the a/l interface. A purely hydrophilic linker (*N*meg) would prefer to associate with the lipid headgroups or aqueous buffered subphase, while inclusion of benzyl chains (*N*pm) could contribute a bulkiness to the linker that could exclude it from any activity-enhancing interactions with the tightly packed lipid film. Interestingly, LC domains largely disappeared at higher Π when any monomer was added, indicating that single aromatic peptoid helices do not support or stabilize LC domains at higher Π, as the dimers do.

The advantages of including 50% aliphatic residues in the linker region are further supported by the PBS adsorption and dynamic cycling data. Although inclusion of **dB1**, **mB2**, **dB2**, and **dB4** led to little to no improvement in adsorptive properties relative to **B1**, both **mB3** and **dB3** enabled a more rapid adsorption of the lipid film, and created surface films that reached a lower γ_{eq} than was seen with the other monomers and disulfide-based dimers. It has been previously shown in peptoid mimics of SP-B that inclusion of aliphatic residues, and in general, an increased proportion of hydrophobicity, facilitated significantly more rapid adsorption to the a/l interface.[42,44] Of the disulfide-based dimers, **dB3** resulted in the lowest γ_{max} and a slightly lower percent SA compression, where the *N*-propyl chains may once again promote better association with the lipid acyl chains of the dynamic film. Overall, the properties of the achiral portion of the peptoid linker did affect the biophysical activity of the lipid-peptoid film, with results pointing to changes in the ability of peptoid to aid in the folding and exclusion of lipids at higher surface pressures, which if inferior, could potentially lead to decreased respreading and higher maximum surface tensions during respiration.

Ultimately, the in vitro dynamic surface activity performance of **dB2c** in a lipid film far surpassed that of any of the disulfide-based dimers or monomers. The triazole moiety is known to be rigid, highly stable, and polar, where nitrogen atoms two and three function as weak hydrogen bond acceptors.[48] The triazole ring is also conformationally more restrictive than a simple disulfide. In previous work, incorporating a triazole amino acid with two flanking methylene groups into a peptoid oligomer caused a hairpin turn, effectively altering the conformation of the structure.[63] We hypothesize that the dramatic improvement in activity could be attributed to the conformational restrictions that this linkage imposes on the terminal peptoid helices and the linking unit. In addition, the late (low) liftoff areas of the **dB2c**-containing film, at both temperatures on the LWSB, support our previous interpretations about dimer exclusion from the lipid film. This could indicate conformational restriction, where the peptoid was physically unable to occupy sufficient area at the interface to affect liftoff. However, it is also possible that the inclusion of four flanking, freely rotatable methylene groups in both the disulfide and triazole linkages may negate the restrictive effect of the triazole group.

Alternatively, the electronic/physical properties of the triazole (an aromatic, electron-donating group) may be another

explanation for the observed increase in surface activity. One could envision associations with the nearby *C*-terminal amide protons or perhaps one of the *N*Lys protons through intra- or intermolecular hydrogen bonding. In addition, the electron-rich triazole ring could be involved in a cation-π interaction with an *N*Lys ammonium cation.[64] Restricted linkage, potential hydrogen bonds, or cation-π interactions could all contribute to lowering the overall entropy of the molecule, and thereby facilitate a helical conformation that more favorably interacts with the anionic lipid headgroups of the lipid-peptoid film, thus enhancing biophysical activity.

From isotherm features alone, the activity of **dB2c** seemed very typical, but FM imaging of the lipid film revealed a significant and unique effect on phase morphology. The difference in LC domain shape at higher temperature, particularly with the formation of well-distributed, elongated rods, and the unusual "attachment" of bright protrusions to the LC domains at both temperatures, indicated a fluidizing effect and a mechanism of material removal from the interface that was distinct from the other lipid-peptoid films. It is also possible that the linkage acts as a polar anchor to the lipid headgroups, unable to insert into the lipid acyl chains, but nonetheless affecting phase morphology. Pursuing a more physiologically mimetic surfactometry technique (PBS) with this molecule revealed excellent adsorptive and dynamic film properties, relative to all other peptoids and established peptide mimics studied. The slightly slower adsorption of the lipid film in the presence of **dB2c** relative to KL_4 can be attributed to the hydrophilic nature of this molecule; perhaps inclusion of 50% *N*-propyl chains would rectify this issue.

Therefore, single, amphipathic, cationic, and aromatic peptoid helices were significantly more affected by a dimerization connectivity that either conformationally or electronically/physically changed the overall structure. From our work, it appears that disulfide-mediated dimerization had little effect on helicity. Single disulfides are known to be fairly flexible, with free rotation of the terminal peptoid helices about the bond. Evidence that conformationally restrictive linkages (like that possible for the triazole-containing linker) improve surface activity is present in the literature, where Raman/ATR-IR of the disulfide bond in dSP-$B_{1\text{-}25}$ vs. dSP-$B_{8\text{-}25}$ (dCys8) demonstrated that inclusion of the flexible SP-$B_{1\text{-}9}$, which flanked the disulfide bond, resulted in a conformational restriction to a higher energy λ(C-SS-C) dihedral angle with increased strain.[30] Although the bond in dSP-$B_{8\text{-}25}$ resided predominantly in a lower energy λ(C-SS-C) conformation, it was determined that inclusion with lipids caused both molecules to favor the conformation adopted by dSP-$B_{1\text{-}25}$[30]. Furthermore, NMR studies of reduced and oxidized "Mini-B" have demonstrated that the two disulfide bonds promoted close, almost parallel association of the helices, and a very amphipathic structure.[32] The reduced form of Mini-B possessed a less defined *C*-terminal helical structure as well.

Although it is not well understood at this time which specific molecular properties of SPs control the stability and activity of a dynamic interfacial surfactant film experiencing cycling of alveolar surface area, it is clear that the same structure-based additions that increased surface activity in peptides may not correspond to increased surface activity in peptoids. The molecular mechanism and structural differences between peptoids and peptides are not sufficiently well-defined to speculate on reasons for disparities in surface activity upon disulfide-mediated dimerization. Two important features missing in peptoids are backbone hydrogen bonding, which is known to stabilize peptide helices, and an overwhelming preference for the trans form in cis/trans isomerization of peptide bonds. The cis conformation in amide bonds linking peptoid residues is known to be more highly populated than in peptides.[65] These two factors could contribute to the increased activity observed after disulfide-mediated dimerization in peptides, where the resulting folded dimeric structure may be more conformationally stable and better able to interact with lipid head groups than its peptoid counterpart. Regardless, we are intrigued by and will continue to investigate the improvements in biologically relevant activity that "click"-mediated dimerization seemed to impose on peptoids for lung surfactant applications, in both in vitro and in vivo environments.

Working toward our broader vision to create a fully functional biomimetic lung surfactant formulation comprising peptoid mimics of SP-B and SP-C, we have created a family of dimerized peptoids that mimic the in vitro surface activity of SP-B by mimicking its specific structural attributes. By exploring dimerization and linker hydrophobicity in these molecules, we have established that (a) dimerization via "click-chemistry" is far more beneficial to surface activity than disulfide-mediated dimerization in peptoids, (b) the potential of peptoids to oligomerize in a hypophase-like environment may explain the lack of activity improvement in disulfide-bonded mimics, and (c) including an achiral, hydrophilic linker with 50% aliphatic residues does render some surface activity improvement. We have provided support for the theory that conformational restriction of secondary and tertiary structure in SP-B may be vital to its biophysical function in the lung. In a broader context, we have demonstrated that "click-chemistry" may be a viable option

for developing natural and non-natural peptide mimics of SPs as well as other biological molecules that primarily operate in a lipid film. The triazole-containing moiety is more rigid and stable and contains more advantageous electronic/physical properties than a disulfide bond, which may render a degree of improved feasibility to drug development in this field. Additionally, this work has further cemented the idea that a completely synthetic, non-natural molecule can adopt structures and exhibit functional physical activity similar to its natural counterparts, which escalates the potential for these molecules to be eventually utilized in a therapeutic setting.

EXPERIMENTAL PROCEDURES

Materials

Peptide and peptoid synthesis reagents and supplies were purchased from Applied Biosystems (ABI) (Foster City, CA) and Sigma-Aldrich (Milwaukee, WI). Fmoc-protected amino acids and resins were purchased from EMD Biosciences (NovaBiochem, San Diego, CA). Primary amines (highest % purity and enantiomeric excess available), di-tert-butyl dicarbonate (Boc), and triphenylmethanol (Trt) were purchased from Sigma-Aldrich. Acetonitrile (ACN), chloroform, methanol, and trifluoroacetic acid (TFA), HPLC grade or better, were purchased from Fisher Scientific (Pittsburgh, PA). All salts were purchased from Fisher Scientific. DPPC and POPG were purchased from Avanti Polar Lipids (Alabaster, AL) and used as received. Palmitic acid (PA) was purchased from Aldrich. Texas Red®, 1,2-dihexadecanoyl-*sn*-glycero-3-phosphoethanolamine, triethylammonium salt (TR-DHPE) was purchased from Molecular Probes (Eugene, OR). All chemicals were used without further purification. Water was Milli-Q 18.2 m$\Omega \cdot$ cm quality.

Peptide and Peptoid Synthesis and Purification

The two peptides, modified SP-$B_{1\text{-}25}$ (Cys8,11 → Ala) and KL_4, were synthesized by standard SPPS[66] Fmoc chemistry on a 0.25 mmol scale using preloaded Wang resin and an ABI 433A automated peptide synthesizer. Peptoids were synthesized by the submonomer method[35] using Rink amide resin, on a 0.25 mmol scale, and an ABI 433A, with Boc protection of *N*-(4-aminobutyl)glycine (*N*Lys), and Trt protection of *N*-(mercaptoethyl)glycine (*N*Cys). All molecules were cleaved from their respective resins by agitation in 90–95% TFA/water (v/v), along with the appropriate scavengers, for 5–10 min (peptoids) to 1 h (peptides). Crude product for purification was obtained by immediate resin filtration of the mixture, dilution with ACN/water, repeated lyophilization, and redissolution in ACN/water. All molecules were purified on a Waters (Waters Corp., Milford, MA) or Varian Prostar (Varian, Inc., Palo Alto, CA) reverse-phase high performance liquid chromatography (RP-HPLC) system with a Grace Vydac (Deerfield, IL), Peeke Scientific (Redwood City, CA), Phenomenex (Torrance, CA), or Varian Dynamax C4 or C18 column, using a linear gradient of percent solvent B in percent solvent A over a selected time period (solvent A is 0.1 percent TFA in water [v/v] and solvent B is 0.1 percent TFA in ACN [v/v]), using standard purification techniques.

Disulfide-dimerized peptoids were synthesized and purified first as monomers. Disulfide-mediated dimerization occurred through 24-h air oxidation in an agitated ACN/water solution, at room temperature, and was monitored by analytical RP-HPLC. The conjugation of peptoid monomers via "click-chemistry" was performed by first synthesizing and purifying the otherwise symmetrical azide and alkyne peptoid monomers (see SI), and then conducting a microwave-assisted "click" reaction (100°C, 1 h) using a Biotage Initiator microwave synthesizer system (Uppsala, Sweden), where known concentrations of both monomers were stirred in *t*-BuOH/H_2O (1:1) containing 5 mol% $CuSO_4 \cdot 5H_2O$ and 15 mol% L-(+)-sodium ascorbate (see SI).[49] The reaction mixture was dialyzed using a Slide-A-Lyzer dialysis cassette (Pierce, Rockford, IL) with a cutoff size of 3.5 kDa, and then RP-HPLC purified. All molecules were obtained in final pure form as a repeatedly lyophilized powder. Final purities were confirmed to be >97% by analytical RP-HPLC and molecular weights were obtained by either electrospray ionization mass spectrometry (ESI/MS) or matrix-assisted laser desorption ionization time of flight mass spectrometry (MALDI-TOF/MS) (Figure 1, inset table).

Surfactant Sample Preparation

The lipids DPPC, POPG, and PA were individually dissolved in a chloroform/methanol solution (3/1 [v/v]) to a known concentration ($\sim$2 or 4 mg mL^{-1}). Single-lipid solutions were then combined by volume at the ratio of DPPC:POPG:PA, 68:22:9 [w:w:w] and to a known total lipid concentration ($\sim$2 mg mL^{-1}). This well-characterized and well-known lipid formulation is considered an adequate mimic of the nonprotein (lipid) fraction of LS.[51] The peptides and peptoids were individually dissolved in methanol from a lyophilized powder to a known concentration (1–2 mg mL^{-1}). For the surfactometry studies, the peptides and peptoids were "spiked" to the lipid mixture at 10 wt% relative to the total lipid content ($\sim$9–10 absolute wt%, see Table I SI), and to a final concentration of $\sim$1 mg lipid mL^{-1}. On the basis of mole % (Table I SI) or calculated number of molecules, there is a roughly equal number of simple monomer unit helices in the **B1** and simple dimer, **dB1**, surfactant samples. Note that previously published work with **B1** at a slightly lower mole percentage (2.16 mol%) resulted in improved PBS static-mode adsorptive properties.[41–43]

LWSB and Epifluorescence Microscopy Studies

Π-A isotherms were obtained using a custom-built LWSB, which has been previously described in detail.[41] The trough was filled with 300 mL of aqueous buffer (150 mM NaCl, 10 mM HEPES, 5 mM $CaCl_2$, pH 6.9) and heated to 25 or 37°C. A Wilhelmy plate (Reigler & Kirstein GMBH, Berlin, Germany) was used to monitor surface pressure and was calibrated in buffer before each run. Each sample was spread at the a/l interface from a chloroform/methanol solution using a glass syringe and allowed to equilibrate for 5–10 min. The barriers were then compressed, expanded, and compressed again at a rate of 30 mm min^{-1}. Isotherm measurements were repeated a total of six times for repeatability and to eliminate effects due to any possibility of leakage. Represented isotherms are first compressions displayed in Figure 2, and averages of important phase transition markers $\pm$ σ are presented in Table I.

To record FM images, a Nikon MM40 compact microscope stand with a 100 W mercury lamp (Tokyo, Japan) was used in conjunction with the Langmuir trough. Epifluorescence was detected by a Dage-MTI three-chip color camera (Dage-MTI, Michigan City, IN) in conjunction with a generation II intensifier (Fryer, Huntley, IL). Samples were spiked with 0.50 mol% TR-DHPE, a fluorescently headgroup-labeled lipid, for detection. Isotherm features remained unchanged after TR-DHPE addition, and presumably, film morphology was largely unchanged by the presence of TR-DHPE at these concentrations. FM images were acquired directly from the compressed film on the a/l interface. Experiments were conducted exactly as the LWSB studies of un-spiked films, with the exception that barrier speed was reduced to 5 mm min^{-1} and experiments were repeated three times for repeatability. Average domain sizes were calculated using ImageJ software (The National Institutes of Health, Bethesda, MD).

Pulsating Bubble Surfactometry

A commercial PBS instrument (General Transco, Largo, FL), modified with a direct, real-time imaging system, which has been previously described and validated in detail,[55] was utilized to obtain both static-mode and dynamic-mode data. Samples were dried from chloroform/methanol 3/1 [v/v] in Eppendorf tubes using a DNA 120 speedvac (Thermo Electron, Holbrook, NY), forming a pellet. The pellet was suspended in buffer (150 mM NaCl, 10 mM HEPES, 5 mM $CaCl_2$, pH 6.9) to 1.0 mg lipid mL^{-1}, with a final volume of $\sim$70 μL. The samples were then mixed with a pipette 20 times, sonicated with a Fisher Model 60 probe sonicator for two 15 second spurts, and then mixed again 20 times to form a dispersed suspension. Samples were then loaded into a small plastic sample chamber (General Transco) using a modified leak-free methodology.[55,67] The sample chamber was then placed in the instrument, surrounded by a water bath held at 37°C. A bubble with a radius of 0.4 mm was then formed, and surface area was monitored throughout the experiment (bubble size gradually increased in both data collection modes, but had a negligible effect on γ).

Static-mode adsorption data were collected for 20 min, where the suspension was allowed to adsorb to the bubble surface over time. Adsorption data were smooth fit to a curve in the Kaleidagraph program by applying a Stineman function to the data, where the output of this function then had a geometric weight applied to the current point and $\pm$10% of the data range to arrive at the smoothed curve (Figure 4). Average $\gamma \pm \sigma$ at selected time intervals are listed in Table II SI. Dynamic-mode data were then subsequently obtained for each sample at the adult respiratory cycle frequency of 20 cpm for 10 min, with a 50% reduction in surface area per pulsation cycle. PBS experiments were repeated six times for each sample to ensure repeatability. Representative PBS loops are presented at five minutes of cycling, and indicate clockwise bubble expansion and counterclockwise compression (Figure 4). Average $\gamma \pm \sigma$ at selected time intervals are presented in Table II. Percent compression is defined here as $100^*[(SA_{max} - SA_{20})/(SA_{max})]$, where SA_{max} was the maximum SA value at expansion, and SA_{20} was the SA at which γ first reaches 20 mN m^{-1} upon compression (Figure 4, inset table).

We gratefully acknowledge Yoriel Marcano, Ann M. Czyzewski, and Michael Connolly, for their valuable assistance, and Mark Johnson for PBS use.

REFERENCES

1. Avery, M. E.; Mead, J. Am J Dis Child 1959, 97, 517–523.
2. Pison, U.; Seeger, W.; Buchhorn, R.; Joka, T.; Brand, M.; Obertacke, U.; Neuhof, H.; Schmit-Nauerburg, K. P. Am Rev Respir Dis 1989, 140, 1033–1039.
3. Lewis, J. E.; Jobe, A. H. Am Rev Respir Dis 1993, 147, 218–233.
4. Robertson, B.; Johansson, J.; Curstedt, T. Mol Med Today 2000, 6, 199–124.
5. Moya, F.; Maturana, A. Clin Perinatol 2007, 34, 145–177.
6. Blanco, O.; Perez-Gil, J. Eur J Pharmacol 2007, 568, 1–15.
7. Mingarro, I.; Lukovic, D.; Vilar, M.; Perez-Gil, J. Curr Med Chem 2008, 15, 393–403.
8. Hawgood, S.; Schiffer, K. Annu Rev Physiol 1991, 53, 375–394.
9. Creuwels, L.; vanGolde, L. M. G.; Haagsman, H. P. Lung 1997, 175, 1–39.
10. Notter, R. H. Lung Surfactants: Basic Science and Clinical Applications; Marcel Dekker: New York, 2000.
11. Veldhuizen, R.; Nag, K.; Orgeig, S.; Possmayer, F. Biochim Biophys Acta 1998, 1408, 90–108.
12. Hall, S. B.; Venkitaraman, A. R.; Whitsett, J. A.; Holm, B. A.; Notter, R. H. Am Rev Respir Dis 1992, 145, 24–30.
13. Schurch, S.; Qanbar, R.; Bachofen, H.; Possmayer, F. Biol Neonate 1995, 67, 61–76.
14. Perez-Gil, J.; Keough, K. M. W. Biochim Biophys Acta 1998, 1408, 203–217.
15. Curstedt, T.; Johansson, J.; Barros-Soderling, J.; Robertson, B.; Nilsson, G.; Westberg, V.; Jornvall, H. Eur J Biochem 1988, 172, 521–525.
16. Vandenbussche, G.; Clercx, A.; Clercx, M.; Curstedt, T.; Johansson, J.; Jornvall, H.; Ruysschaert, J. M. Biochemistry 1992, 31, 9169–9176.
17. Andersson, M.; Curstedt, T.; Jornvall, H.; Johansson, J. FEBS Lett 1995, 362, 328–332.
18. Hawgood, S.; Derrick, M.; Poulain, F. Biochim Biophys Acta 1998, 1408, 150–160.
19. Clark, J. C.; Wert, S. E.; Bachurski, C. J.; Stahlman, M. T.; Stripp, B. R.; Weaver, T. E.; Whitsett, J. A. Proc Natl Acad Sci USA 1995, 92, 7794–7798.
20. Ikegami, M.; Whitsett, J. A.; Martis, P. C.; Weaver, T. E. Am J Physiol Lung Cell Mol Physiol 2005, 289, L962–L970.
21. Cochrane, C. G.; Revak, S. D. Science 1991, 254, 566–568.
22. Waring, A.; Taeusch, H. W.; Bruni, R.; Amirkhanian, J. D.; Fan, B. R.; Stevens, R.; Young, J. Pept Res 1989, 2, 308–313.
23. Bruni, R.; Taeusch, H. W.; Waring, A. J. Proc Natl Acad Sci USA 1991, 88, 7451–7455.
24. Baatz, J. E.; Sarin, V.; Absolom, D. R.; Baxter, C.; Whitsett, J. A. Chem Phys Lipids 1991, 60, 163–178.
25. Revak, S. D.; Merritt, T. A.; Hallman, M.; Heldt, G.; Lapolla, R. J.; Hoey, K.; Houghten, R. A.; Cochrane, C. G. Pediatr Res 1991, 29, 460–465.
26. Booth, V.; Waring, A. J.; Walther, F. J.; Keough, K. M. W. Biochemistry 2004, 43, 15187–15194.

27. Veldhuizen, E. J. A.; Waring, A. J.; Walther, F. J.; Batenburg, J. J.; van Golde, L. M. G.; Haagsman, H. P. Biophys J 2000, 79, 377–384.
28. Walther, F. J.; Hernandez-Juviel, J. M.; Gordon, L. M.; Sherman, M. A.; Waring, A. J. Exp Lung Res 2002, 28, 623–640.
29. Bringezu, F.; Ding, J. Q.; Brezesinski, G.; Waring, A. J.; Zasadzinski, J. A. Langmuir 2002, 18, 2319–2325.
30. Biswas, N.; Waring, A. J.; Walther, F. J.; Dluhy, R. A. Biochim Biophys Acta 2007, 1768, 1070–1082.
31. Waring, A. J.; Walther, F.; Gordon, L. M.; HernandezJuviel, J.; Hong, T.; Sherman, M. A.; Alonso, C.; Alig, T.; Brauner, J. W.; Bacon, D.; Zasadzinski, J. J Pept Res 2005, 66, 364–374.
32. Sarker, M.; Waring, A. J.; Walther, F. J.; Keough, K. M. W.; Booth, V. Biochemistry 2007, 46, 11047–11056.
33. Miller, S. M.; Simon, R. J.; Ng, S.; Zuckermann, R. N.; Kerr, J. M.; Moos, W. H. Drug Dev Res 1995, 35, 20–32.
34. Kirshenbaum, K.; Barron, A. E.; Goldsmith, R. A.; Armand, P.; Bradley, E. K.; Truong, K. T. V.; Dill, K. A.; Cohen, F. E.; Zuckermann, R. N. Proc Natl Acad Sci USA 1998, 95, 4303–4308.
35. Zuckermann, R. N.; Kerr, J. M.; Kent, S. B. H.; Moos, W. H. J Am Chem Soc 1992, 114, 10646–10647.
36. Wu, C. W.; Sanborn, T. J.; Zuckermann, R. N.; Barron, A. E. J Am Chem Soc 2001, 123, 2958–2963.
37. Sanborn, T. J.; Wu, C. W.; Zuckermann, R. N.; Barron, A. E. Biopolymers 2002, 63, 12–20.
38. Armand, P.; Kirshenbaum, K.; Goldsmith, R. A.; Farr-Jones, S.; Barron, A. E.; Truong, K. T. V.; Dill, K. A.; Mierke, D. F.; Cohen, F. E.; Zuckermann, R. N.; Bradley, E. K. Proc Natl Acad Sci USA 1998, 95, 4309–4314.
39. Wu, C. W.; Kirshenbaum, K.; Sanborn, T. J.; Patch, J. A.; Huang, K.; Dill, K. A.; Zuckermann, R. N.; Barron, A. E. J Am Chem Soc 2003, 125, 13525–13530.
40. Wu, C. W.; Seurynck, S. L.; Lee, K. Y. C.; Barron, A. E. Chem Biol 2003, 10, 1057–1063.
41. Seurynck, S. L.; Patch, J. A.; Barron, A. E. Chem Biol 2005, 12, 77–88.
42. Seurynck-Servoss, S. L.; Dohm, M. T.; Barron, A. E. Biochemistry 2006, 45, 11809–11818.
43. Seurynck-Servoss, S. L.; Brown, N. J.; Dohm, M. T.; Wu, C. W.; Barron, A. E. Coll Surf B Biointerfaces 2007, 57, 37–55.
44. Brown, N. J.; Wu, C. W.; Seurynck-Servoss, S. L.; Barron, A. E. Biochemistry 2008, 47, 1808–1818.
45. Chongsiriwatana, N. P.; Patch, J. A.; Czyzewski, A. M.; Dohm, M. T.; Ivankin, A.; Gidalevitz, D.; Zuckermann, R. N.; Barron, A. E. Proc Natl Acad Sci USA 2008, 105, 2794–2799.
46. Kolb, H. C.; Finn, M. G.; Sharpless, K. B. Angew Chem Int Ed 2001, 40, 2004–2021.
47. Holub, J. M.; Jang, H. J.; Kirshenbaum, K. Org Biomol Chem 2006, 4, 1497–1502.
48. Kolb, H. C.; Sharpless, K. B. Drug Discovery Today 2003, 8, 1128–1137.
49. Li, J.; Zheng, M. Y.; Tang, W.; He, P. L.; Zhu, W. L.; Li, T. X.; Zuo, J. P.; Liu, H.; Jiang, H. L. Bioorg Med Chem Lett 2006, 16, 5009–5013.
50. Moses, J. E.; Moorhouse, A. D. Chem Soc Rev 2007, 36, 1249–1262.
51. Tanaka, Y.; Takei, T.; Aiba, T.; Masuda, K.; Kiuchi, A.; Fujiwara, T. J Lipid Res 1986, 27, 475–485.
52. Cochrane, C. G.; Revak, S. D.; Merritt, A.; Heldt, G. P.; Hallman, M.; Cunningham, M. D.; Easa, D.; Pramanik, A.; Edwards, D. K.; Alberts, M. S. Am J Respir Crit Care Med 1996, 153, 404–410.
53. Moya, F. R.; Gadzinowski, J.; Bancalari, E.; Salinas, V.; Kopelman, B.; Bancalari, A.; Kornacka, M. K.; Merritt, T. A.; Segal, R.; Schaber, C. J.; Tsai, H.; Massaro, J.; d'Agostino, R. Pediatrics 2005, 115, 1018–1029.
54. Bernardino de la Serna, J.; Perez-Gil, J.; Simonsen, A. C.; Bagatolli, L. A. J Biol Chem 2004, 279, 40715–40722.
55. Seurynck, S. L.; Brown, N. J.; Wu, C. W.; Germino, K. W.; Kohlmeir, E. K.; Ingenito, E. P.; Glucksberg, M. R.; Barron, A. E.; Johnson, M. J Appl Physiol 2005, 99, 624–633.
56. Lee, K. Y. C.; Lipp, M. M.; Zasadzinski, J. A.; Waring, A. J. Coll Surf A Physicochem Eng Aspects 1997, 128, 225–242.
57. Serrano, A. G.; Cruz, A.; Rodriguez-Capote, K.; Possmayer, F.; Perez-Gil, J. Biochemistry 2005, 44, 417–430.
58. Beck, D. C.; Ikegami, M.; Na, C. L.; Zaltash, S.; Johansson, J.; Whitsett, J. A.; Weaver, T. E. J Biol Chem 2000, 275, 3365–3370.
59. Zaltash, S.; Griffiths, W. J.; Beck, D.; Duan, C. X.; Weaver, T. E.; Johansson, J. Biol Chem 2001, 382, 933–939.
60. Ahn, V. E.; Faull, K. F.; Whitelegge, J. P.; Fluharty, A. L.; Prive, G. G. Proc Natl Acad Sci USA 2003, 100, 38–43.
61. Wang, Y. D.; Rao, K. M. K.; Demchuk, E. Biochemistry 2003, 42, 4015–4027.
62. Ryan, M. A.; Qi, X.; Serrano, A. G.; Ikegami, M.; Perez-Gil, J.; Johansson, J.; Weaver, T. E. Biochemistry 2005, 44, 861–872.
63. Pokorski, J. K.; Jenkins, L. M. M.; Feng, H.; Durell, S. R.; Bal, Y.; Appella, D. H. Org Lett 2007, 9, 2381–2383.
64. Mecozzi, S.; West, A. P.; Dougherty, D. A. Proc Natl Acad Sci USA 1996, 93, 10566–10571.
65. Sui, Q.; Borchardt, D.; Rabenstein, D. L. J Am Chem Soc 2007, 129, 12042–12048.
66. Merrifield, R. B. J Am Chem Soc 1963, 85, 2149–2154.
67. Putz, G.; Goerke, J.; Taeusch, H. W.; Clements, J. A. J Appl Physiol 1994, 76, 1425–1431.